# PCCP

Accepted Manuscript






ROYAL SOCIETY OF CHEMISTRY

rsc.li/pccp

View Article Online
DOI: 10.1039/C9CP01611B

# Reaction Mechanism and Kinetics for Ammonia Synthesis on the Fe(211) Reconstructed Surface

Jon Fuller[1], Alessandro Fortunelli[2,3*], William A. Goddard[2*], and Qi An[1*]

[1]Department of Chemical and Materials Engineering, University of Nevada – Reno, Nevada 89577, United States
[2]Materials and Procs Simulation Center (MSC), California Institute of Technology, Pasadena, California 91125, United States
[3]CNR-ICCOM, Consiglio Nazionale delle Ricerche, THC2-Lab, Pisa, 56124, Italy



## ABSTRACT

To provide guidelines to accelerate the Haber-Bosch (HB) process for synthesis of ammonia from hydrogen and nitrogen, we used Quantum Mechanics (QM) to determine the reaction mechanism and free energy reaction barriers under experimental reaction conditions (400°C and 20 atm) for all 10 important surface reactions on the Fe(211)R surface. These conditions were then used in full kMC modeling for 30 minutes to attain steady state. We find that the stable surface under Haber-Bosch conditions is the missing row 2x1 reconstructed surface (211)R and that the Turn Over Frequency (TOF) is 18.7/sec per 2x2 surface site for 1.5 torr $NH_3$ pressure, but changes to 3.5/sec for 1 atm, values close (within 6%) to the ones on Fe(111). The experimental ratio between (211) and (111) rates at low (undisclosed) $NH_3$ pressure was reported to be 0.75. The excellent agreement with experiment on two very different surfaces and reaction mechanisms is a testament of the accuracy of QM modeling. In addition, our kinetic analysis indicates that Fe(211)R is more active than Fe(111) at high pressure, close to HB industrial conditions, and that (211)R is more abundant than (111) via a steady-state Wulff construction under HB conditions. Thus, at variance with common thinking, we advocate the Fe(211)R surface as the catalytically active phase of pure iron ammonia synthesis catalyst under HB industrial conditions.

View Article Online
DOI: 10.1039/C9CP01611B





## INTRODUCTION

The Haber-Bosch (HB) process has become a most important chemical manufacturing process in the world, being used to produce over 150 million tons of ammonia ($NH_3$) in 2017.[1] This process converts nitrogen gas ($N_2$) from the atmosphere along with hydrogen gas ($H_2$) extracted from natural gas or other sources into ammonia using an Fe based metal catalyst and subjected to high temperature and pressure to accelerate the dissociation of $N_2$ into monatomic nitrogen. Since the HB process must reach both high temperatures and high pressures to effectively produce $NH_3$, the efficiency of HB is a key concern. Industrial production typically uses iron catalysts and claim an efficiency of up to 70% through use of temperatures of up to 850 K in tandem with pressures of up to 200 atm.[2,3] These temperature and pressure conditions increase the capital costs of the plants and make the energy consumption by the industrial application of HB process a significant portion of the world's total power output (up to 2%). This motivates the search for novel catalysts to increase the efficiency and cost of the Haber-Bosch process. Here we follow the strategy of deriving precise quantum mechanics (QM) information on full reaction energy diagram of a catalytic process to understand mechanistic aspects in detail and make them the basis for rational design of improved systems on which experiment can then focus on.

Early experimental work in $NH_3$ synthesis on the Fe catalyst was performed by Spencer et al[4] with further explanation by Ertl of the nature of the $NH_3$ synthesis mechanism.[5] An extensive summary of $NH_3$ synthesis rates on various Fe surfaces was compiled by Somorjai and co-workers[6] from own prior research who showed that the Fe(111) and Fe(211) surfaces are the most catalytically active iron surfaces. Experimental work on various Fe surfaces performed by Somorjai et. al. utilized Low-Energy Electron Diffraction (LEED) and Atomic Emission Spectroscopy (AES) to evaluate both the reaction mechanisms and rates of reaction, which they concluded to be reliant upon high-coordination and exposed second or third layer sites. Higher reaction rates occurring on tiered surfaces such as that found in the Fe(211) missing-row reconstructed surface, which is the focus of this research, is well documented.[7] The experimental rates under undisclosed conditions on the Fe(111) and Fe(211) surfaces were 1.3 x $10^{-8}$ moles-$NH_3$/cm$^2$/sec and 0.97 x $10^{-8}$ moles-$NH_3$/cm$^2$/sec, respectively, so that Fe(211) is 25% slower. However, both were much higher than for Fe(100) and Fe(210) which were 0.18 x $10^{-8}$ and 0.15 x $10^{-8}$ moles-$NH_3$/cm$^2$/sec.[8,9] A dramatic improvement in the efficiency of the Fe catalyst is needed to reduce the huge energy costs, making it important to determine the reaction mechanism.

Previously we carried out very extensive Quantum Mechanics (QM) calculation on the Fe(111) surface, leading to 26 configurations for the 2x2 surface that play an important role at the Somorjai reaction conditions of 400 °C and 20 atm total pressure of reactants in stoichiometric ratio.[10] We predicted the free energies and free energy reaction rates for all 10 important reaction steps at these conditions which we used in a 2 × $10^9$-steps kinetic Monte Carlo (kMC) simulation to predict a TOF = 17.7 molecules-$NH_3$/sec per 2x2 site in excellent agreement with the experimental value of 9.7 molecules-$NH_3$/sec per 2x2 site at 1.5 torr $NH_3$ pressure.

We report here QM based studies on the Fe(211) surface that we used to predict the reaction mechanism and free energy reaction kinetics for all 10 important surface reactions and all 24

View Article Online
DOI: 10.1039/C9CP01611B





important surface adsorbates configurations important to the full reaction pathway for synthesis of $NH_3$. This was carried out at the same level as for Fe(111), including the free energy barriers that limit the rates of reaction under the prescribed conditions. We show that the missing row 2x1 reconstructed surface is stable under reaction conditions, confirming earlier predictions. We used the predicted barriers in a kinetic Monte Carlo (kMC) model to predict the steady state rates of all reaction steps leading to a turnover frequency (TOF) of 18.7/sec per 2x2 surface site at 1.5 torr $NH_3$ and 3.45/sec at 1 atm $NH_3$. This leads to an effective overall barrier of 1.68 eV for the Fe(211) missing row surface or Fe(211)R at steady-state working conditions of T = 673 K; $P_{N2}$ = 5 atm, $P_{H2}$ = 15 atm and $P_{NH3}$ = 1 atm, which can be compared to 1.67 eV for (111). More interesting, the HB catalytic activity of Fe(211)R becomes significantly larger than (111) over a wide range of conditions, particularly when close to industrial HB conditions, and the steady-state energy of Fe(211)R is lower than Fe(211) so it is expected to be more abundant under reaction conditions on the basis of a steady-state Wulff construction. Thus, we expect that Fe(211)R is the prevailing catalytically active phase in the industrial HB process on pure Fe catalysts.

## COMPUTATIONAL METHODS

### Periodic QM models

Our QM studies use the Perdew-Burke-Ernzerhof (PBE)[11,12] functional of Density Functional Theory (DFT) along with the D3 (Becke-Johnson)[13] corrections for the van der Waals London dispersion interaction. The VASP[14-16] software package was used for all the periodic calculations.

To compute the surface energy accurately, we constructed slab models of Fe(211) and Fe(111) surfaces with 13 layers of Fe atoms periodically arrayed for a 2x2 unit cell. The middle layer was fixed, and other 12 layers allowed to relax, obtaining equivalent top and bottom layers. To obtain the Fe(211) missing row reconstructed configuration, we removed two atoms along the $[\bar{1}11]$ direction on the top and bottom surfaces of Fe(211). This method agrees with prior computational results for pure Fe surfaces.[10]

To examine the surface reactions on the Fe(211) reconstructed surface, denoted (211)R, we used a slab with six layers of Fe atoms arranged periodically in a (2x2) (6.912 x 8.276 $A^2$) unit cell with four atoms per layer but two surface Fe per cell due to the missing row reconstruction. We included 15 Å of vacuum in the z direction to prevent interactions between surface molecules and the replicated cells. We allowed the top three layers of Fe atoms to relax while the lower three layers were fixed to maintain the optimal geometry required to simulate bulk Fe.[10]

The Energy cutoff was set to 600 eV for all calculations. The convergence criteria for forces and energies were set to 1.0 x $10^{-3}$ eV/ Å, and 1.0 x $10^{-6}$ eV, respectively, using K-point sampling of 4 x 4 x 1. All calculations were included spin-polarization. Our previous QM studies on the Fe(111) surface which led to excellent agreement with single crystal Fe(111) experiments used exactly the same parameters.[10]

View Article Online
DOI: 10.1039/C9CP01611B



Geometry optimization and phonon calculations were performed using the same convergence threshold for energy and force to ensure reliable phonon frequencies without negative eigenvalues. The free energy of each state was obtained as previously using established methods[8] for both minima and transition states.

Transition states were found using the climbing Nudged Elastic Band (NEB) method included in VASP-VTST[18] by first finding initial and final states for each transition using geometry optimization. Each NEB calculation included eight intermediate images between the optimized initial and final states in which the adsorbed surface species was allowed to move. A true transition state from each NEB was found using phonon calculations to show a single negative value in the Hessian.[18] To accuracy locate the transition state structure, the Dimer calculation was performed based on the NEB results. The frequency was examined after the Dimer calculations to confirm the TS are the true TS structure. Phonon calculations were performed on transition state structures to accurately calculate free energies.

**Finite molecule QM model**

All calculations for small gas molecules in this research were made with the PBE-D3 functional. The zero-point energy (ZPE), enthalpy (H) and entropy (S) were obtained at a specified temperature (T) using this method and a total free energy correction was calculated according to G = H – TS. This was in turn added to the energy obtained via DFT to provide the total free energy of the molecule. The free energy was corrected for pressure by treating the molecule as an ideal gas at reference pressure P = 1 atm by adding $RT \times \ln(P_2/P_1)$. With respect to our previous study on the Fe(111) surface here we use consistently the VASP code also for evaluating entropic corrections for free molecules, instead of the Jaguar code.[10]

## RESULTS AND DISCUSSION

### Surface Energy

The Fe(211)R surface (Fig. 1) with the missing row-type reconstruction was investigated based on prior studies that indicated surfaces with exposed potential sites for adsorption below the surface layer were more catalytically active.[6] The missing row surface reconfiguration as reported in prior work exposes the sites in both the second and third layer for potential molecular adsorption.[19] The surface energy for the Fe(211)R surface was calculated according to:

$$E_{surface} = E_{top} + E_{bottom} = (E_{slab} - N*E_{bulk/atom}) / A \qquad (1)$$

Free energy comparisons of the two surfaces indicated comparable surface energy for the Fe(211)R surface (3.425 J/m$^2$) when compared to the normal Fe(211) surface (3.300 J/m$^2$) and the Fe(111) surface (3.233 J/m$^2$) at T = 0 K. However, our QM studies show that with adsorbed nitrogens under reaction conditions, the Fe(211)R surface (1.912 J/m$^2$) is significantly more stable than either the normal Fe(211) surface (2.418 J/m$^2$) or the well-studied Fe(111) surface (2.127 J/m$^2$).[6,20,21] This is because of the N binding to the third-layer sites in the trough region, as shown for the 4N configuration in Fig. S1 of Supplemental Information (SI). Reconstruction testing with four adsorbed H atoms also indicates that the Fe(211)R surface is energetically

View Article Online
DOI: 10.1039/C9CP01611B



preferable compared to the unreconstructed Fe(211) surface with excellent agreement with previous research.

**Surface Binding Sites**

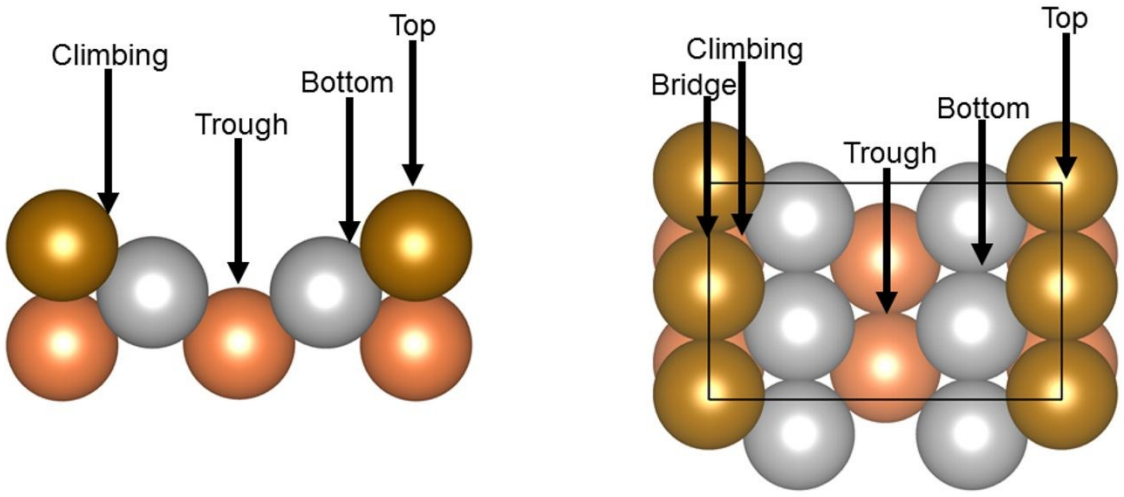


**Fig. 1** - Structure of the Fe(211)R surface with various adsorption sites indicated. Adsorption sites are shown from the top and side view for clarity. Only the top three layers (of six) are shown. For the example adsorption sites pictured above: the top site corresponds to (1.0, 0.0, 0.50), the bottom site corresponds to (0.69, 0.14, 0.36), the climbing site corresponds to (0.63, 0.58, 0.44), the bridge site corresponds to (0.7, 1.0, 0.44) and the trough site corresponds to (0.59, 0.50, 0.31).

Adsorption sites for H, N, NH, $NH_2$ and $NH_3$ were found to be in rough accord with previous theoretical work.[24] Due to the missing row surface reconfiguration, the Fe(211)R surface used in this research has five primary sites for an adsorbate to bond at:

- the first layer Fe atoms (top) with adsorbed species bonding at roughly 2.09 Å above a top layer Fe atom,
- between two first layer Fe atoms (bridge) with adsorbed species bonding at roughly 1.71 Å from each top layer Fe atom,
- a raised site parallel to the first-layer ridge atoms (climbing) with adsorbed species bonding roughly 1.91 Å from adjacent top layer Fe atom and 2.01 Å from second layer Fe atom,
- a shallow 3-fold site in the second layer (bottom) with adsorbed species bonding at roughly 1.81~2.00 Å from adjacent Fe atoms and
- a 4-fold site in the third layer (trough) with adsorbed species bonding at roughly 1.83~1.90 Å from adjacent Fe atoms.

We also found intermediate sites to be active for some molecules, particularly between the bottom and climbing sites.

We found the following preferred positions and adsorption energies for the various species:

View Article Online
DOI: 10.1039/C9CP01611B



- H prefers the bridge (0.71 eV) and top sites (0.62-0.70eV),
- N prefers the bottom sites (1.06 eV) and the trough sites (1.53 eV),
- NH prefers the bottom site with the H opposite the first layer Fe atoms to minimize vdW repulsion (0.92 eV),
- $NH_2$ prefers the climbing site (0.70 eV), and
- $NH_3$ prefers the top site (0.49 eV).

These sites and their adsorption energy are compared with previous theory using the PW-91 functional[24] in Table S1 of SI. Note that the previous PW-91 simulations were on the unreconstructed Fe(211) surface.

A primary difference in the Fe(211)R surface from the unreconstructed Fe(211) surface is the presence of a "trough" from the missing first layer Fe row. For the unreconstructed Fe(211) surface all N and H atoms can participate in the reaction pathway and can desorb from the surface as needed. In the Fe(211)R missing row configuration, we found it to be energetically unfavorable for the trough-position N atoms to participate in the reaction pathway once adsorbed. Additionally, this missing row region changes the preferred binding site for the $NH_2$ species to a climbing position between the bottom and top positions on the Fe(211)R surface since there is no middle ridge of atoms to form a bridge position observed in the Fe(211) surface.

**Energy Landscape for $3H_2 + N_2 \Rightarrow 2NH_3$ and mechanisms of reaction, with illustrations**

Here we first consider the reaction energy diagram at the steady working conditions of T = 673 K, P = 20 atm, and P($NH_3$) = 1 atm, as shown in Fig. 2, where the barriers of the different reaction steps are highlighted in different colors according to their chemical character, i.e., H-migration = green, N2-adsorption/dissociation = yellow, NH3 desorption = red, H2-poisoning = blue.

View Article Online
DOI: 10.1039/C9CP01611B



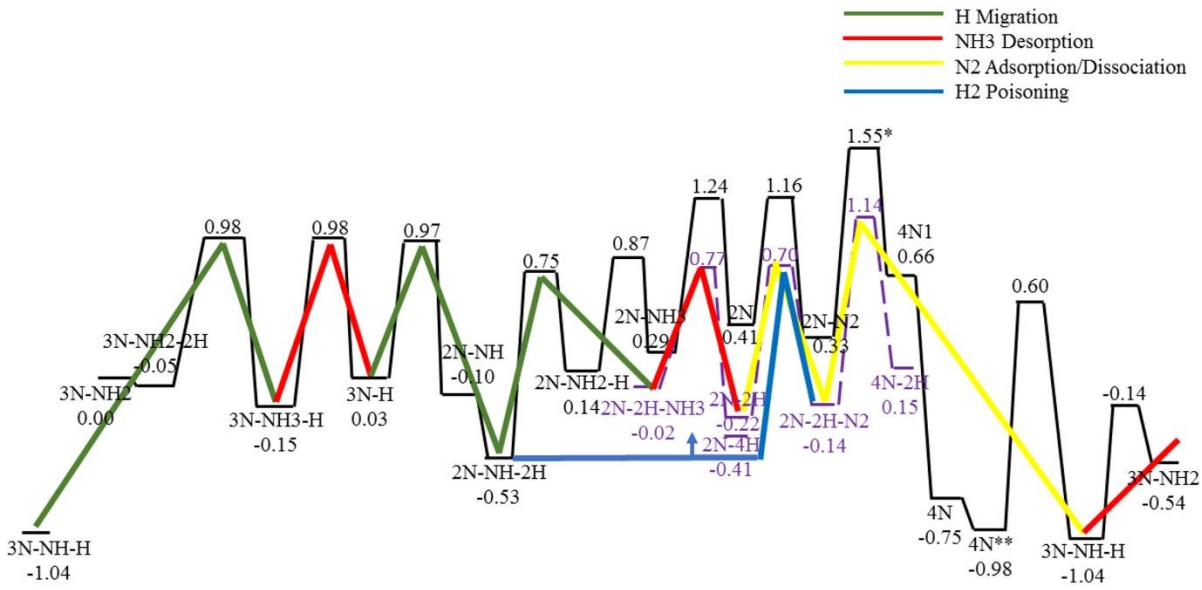


**Fig. 2 –** Fe(211)R $NH_3$ synthesis free energy diagram at 673K, $P(H_2)$ = 15 atm, $P(N_2)$ = 5 atm, and $P(NH_3)$ = 1 atm. ΔG is in eV; 3N-$NH_2$ is used as the reference state. An alternate pathway with 2H added to surface is proposed in purple with lower barriers. The tricolored line added for clarity illustrates the energy barriers for the reaction along with the associated process on the surface, with green corresponding to H migration, red corresponding to $NH_3$ desorption, and yellow corresponding to $N_2$ adsorption and dissociation steps. The blue line indicates $H_2$ poisoning, with the energy relation to the 2N-NH-2H state shown. The complex path for $N_2$ dissociation is not shown. **ΔG is shown for lowest step in 4N ridge diffusion process.

## 1. Explanation and Reference State

We performed density functional theory (DFT) calculations using the Perdew-Burke-Ernzerhof (PBE-D3)[11-12] functional with H, N, NH, $NH_2$, and $NH_3$ molecules arranged at varying adsorption sites on the Fe(211)R surface. These adsorption sites were found to be the most stable under reaction conditions. DFT geometry optimization was carried out for all adsorbed molecules for all 24 surface configurations found to be stable under reaction conditions. We then calculated reaction barriers for the main and alternate considered reaction pathways for $NH_3$ synthesis. For both pathways, the lowest free energy barrier was sought.

In this section we will discuss free energies at a total pressure P = 21 atm with $H_2$ pressure of 15 atm, $N_2$ pressure of 5 atm, and $NH_3$ pressure of 1 atm. The temperature is (T = 673 K, corresponding to the single crystal experiments) drastically lower than the extreme conditions of industrial ammonia synthesis (HB) process, typically held at 773-823 K and total pressure of 150-250 atm. Other conditions will be investigated in the kinetic model in the next section.

View Article Online
DOI: 10.1039/C9CP01611B



We used the 3N_$NH_2$ surface configuration as the reference state for constructing the synthesis pathway, just as for the Fe(111) surface. We designate the free energy for this state to be G = 0 for this paper.

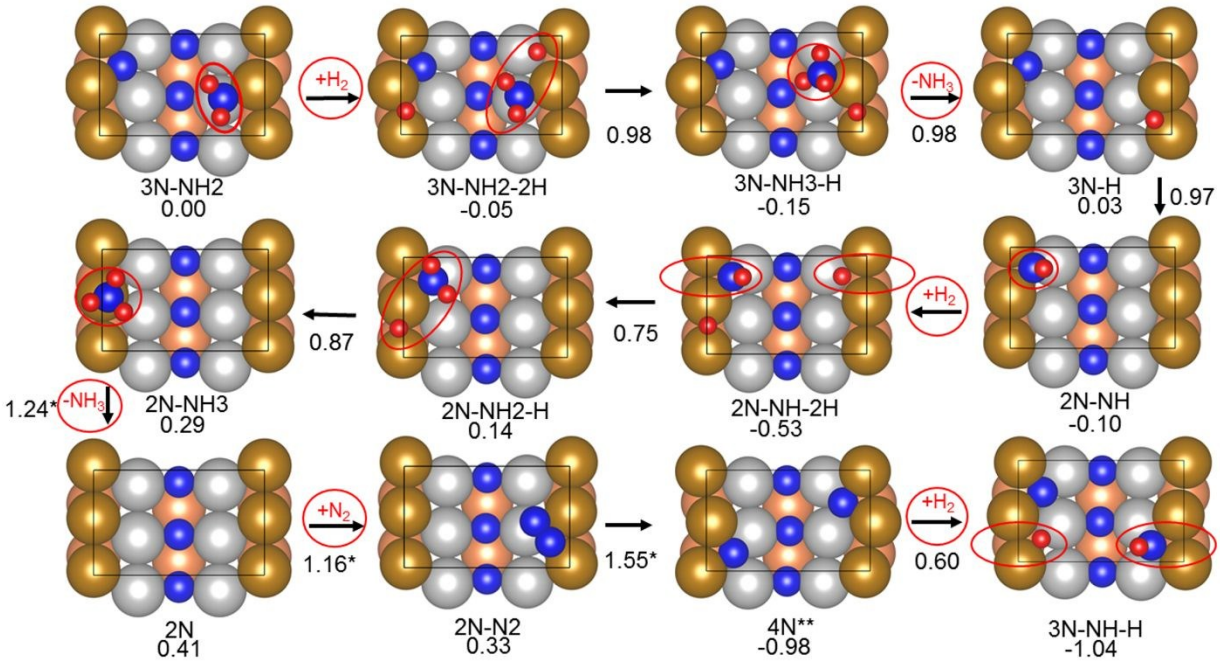


**Fig. 3 –** Main reaction pathway for $NH_3$ synthesis on the Fe(211)R surface. The reported ΔG in eV is relative to the 3N-$NH_2$ reference state. The primary reactive species for each state is circled in red for clarity. Likewise, adsorption or desorption of species is circled between states. Here * indicates an alternative pathway presented for these steps to minimize reaction barriers. Complex. 2N-$N_2$ -> 4N** pathway is presented in Fig. S4 of the SI.

## 2. Reaction pathway

The primary configurations of the reaction pathway are presented in Fig. 3, consisting of 12 main states and 11 transition states (using the NEB technique[13] with DIMER calculations applied for nebulous cases) each verified by the presence of a single negative value in the Hessian. Various alternative pathways were also examined in our search to lower the highest reaction barriers beginning with the desorption of $NH_3$ from the surface prior to the steps of restoring the 4N state for continuity of the pathway. The addition of 2H to the surface was found to significantly lower the overall reaction barrier; this alternate pathway is discussed below and in detail in the SI. The detailed reaction pathway is discussed in section 3 and Fig. S2-S6 of the SI, with the alternate reaction pathway found to minimize the energy barriers of the reaction found in section 4 and Fig. S7-S8 of the SI.

We focus on the Langmuir-Hinshelwood (LH) reaction mechanism for the formation of $NH_x$ species on the surface from adsorbed H and N, the reduction and dissociation of the triple bond for the adsorbed $N_2$ to restore to the 4N state, along with $NH_3$ and $N_2$ desorption processes. $H_2$ dissociative desorption was calculated to have a minimal barrier for all steps and is thus omitted.

View Article Online
DOI: 10.1039/C9CP01611B



Details on bond lengths and adsorption energies for the species discussed below are included in Table S1 of the SI. We discuss these three reaction mechanisms in details below.

**a. H migration**

The LH mechanism has been well-documented in prior research[25,26] and we find it to be the primary mechanism involved in $NH_x$ production on Fe(211)R, with the Eley-Rideal mechanism playing a role in specific steps. $H_2$ atoms easily dissociate and adsorb to the surface on top and bridge sites and then migrate across the surface to form $NH_x$ species consistent with the LH mechanism, as shown in Fig 3. H migration to form $NH_x$ has lower barriers for the overall reaction than the other reaction mechanisms.

**b. $NH_3$ desorption**

The $NH_3$ desorption process is relatively simple in comparison to other reaction mechanisms. The $NH_3$ molecule assumes a top position bonded to a single Fe in the first layer, consistent with previous theoretical research,[24] before detaching to enter the gaseous portion of the system once enough energy is added to the system. The second $NH_3$ desorption represents the secondary overall reaction barrier outside of the 2N-$N_2$ to 4N restoration process with the included transitions and $N_2$ desorption barriers.

**c. $N_2$ dissociation/adsorption/desorption**

$N_2$ adsorption/dissociation steps contribute significantly to the overall energy barrier in the main reaction pathway. $N_2$ adsorbs to the surface initially in a vertical (perpendicular) configuration at a top site to minimize repulsive interactions with adsorbed N atoms in the trough region. $N_2$ desorption is involved in each subsequent state as the $N_2$ migrates to the bottom site, then assumes an orientation parallel to the surface and tilted towards the first-layer Fe ridge. We found the $N_2$ molecule adsorption to the top position to be the tertiary barrier to the overall reaction, with the transition of the $N_2$ molecule to the bottom site being the quaternary overall energy barrier for the synthesis pathway. The $N_2$ movement between sites and dissociation process is shown in more detail in Fig. S9 of the SI.

**d. $H_2$ poisoning/evolution**

We finally stress that "hydrogen poisoning/evolution" can also become potentially rate-determining. A hydrogen poisoning effect has indeed been previously found for Rh 1$^{st}$-layer doping of the Fe(111)surface.[43]. It corresponds to the possibility that the $H_2$ molecule adsorb dissociatively on the empty sites of the Fe catalyst in competition with the $N_2$ molecule, thus preventing $N_2$ to absorb and dissociate, and that the energy of the associated configuration (in the present case, the 2N-4H configuration) is lower in free-energy than that of the 2N-NH-2H state, therefore effectively slowing down the catalytic process, i.e., poisoning the catalyst.

**Comparison with previous studies**

View Article Online
DOI: 10.1039/C9CP01611B



The predicted overall barrier on the Fe(211) non-reconstructed surface from previous theoretical research is 1.67 eV[24] represented by the $NH_2$ + H -> $NH_3$ dissociation step, in contrast to our overall predicted barrier of 1.14 eV on the Fe(211)R surface for this step. This is partially due to the presence of additional second and third layer adsorption sites on the Fe(211)R surface which provide an overall more favorable reaction pathway[6]; addition of 2H species also significantly lowers barriers in the $N_2$ dissociation process and second $NH_3$ desorption from the surface.

Previous theoretical research utilizing QM methods for the Fe(211) surface has focused on the non-reconstructed surface.[24] However, other studies have indicated Fe surfaces with exposed deep-layer sites sustain the greatest reaction efficiency[6,28,29] under industrial conditions, such as the relatively well-examined Fe(111) surface which contains exposed adsorption sites on the second and third Fe layers. Following this concept, this research seeks to explore the reaction mechanism and rates of reaction on the Fe(211) surface which has undergone missing row-type reconstruction due to the presence of hydrogen and nitrogen on the surface at industry standard temperatures and pressures, the presence and mechanism of which has been explored in previous experimental and theoretical research.[29-31] Due to the additional exposure of subsurface layers as potential adsorption sites for the $NH_3$ synthesis pathway, we believed that the mostly-unexplored missing row reconstruction would prove to have lower overall barriers for the reaction than the unreconstructed surface.[6]

Research into catalyst design for improving efficiency has taken increased priority in recent years, with extensive research into surface promotion using various alkali species on and embedded into the Fe(111)[32] and Fe(211)[33] surfaces along with research into alternative ruthenium catalysts.[34,35] Understanding the full reaction mechanism is of key importance to designing a catalytic surface for the Haber-Bosch reaction – to date, most work has focused on the Fe(111) surface as the most active surface and less work has been completed on the second-most-active Fe(211) surface.[6] We believe that understanding the synthesis mechanism for ammonia on the Fe(211) surface is important for providing a baseline of knowledge for future catalyst design to improve the efficiency of the Haber-Bosch process.

**Spin comparison and changes in magnetic moment**

Since the Fe(211)R surface is ferromagnetic, magnetic moment and spin changes are relevant to the energetics of the reaction mechanism. The Magnetic moment comparison and spin analysis was carried out for the 2N-N2 -> 4N(initial) and 2N-2H-N2 -> 4N-2H dissociation processes which represent the highest overall barrier for the whole reaction path. The total magnetic moment (μB) was found to decrease in relation to that of the Fe(211)R surface which is consistent with prior Fe111 surface,[10] as shown in Table 1. This is due to the spin reduction from coupling due to covalent valence bond formation of N to surface Fe atoms to facilitate breaking of the NN bonds as the dissociation proceeds. Surface Fe atoms show a decrease in spin and an increase in charge as they bond to N as seen in Fig. S10 of SI. These trends correlate with the results of previous research and help support the spin-coupling bonding theory for surface adsorbates.[36-39] The Bond length of the adsorbed $N_2$ species notably changes from 1.14 Å in the initial state for both pathways to a length of 1.71 Å in the transition states, indicating reduction from a double bond to an elongated single bond prior to dissociation which further supports the

View Article Online
DOI: 10.1039/C9CP01611B



observed changes in spin and charge for the corresponding surface Fe atoms. Little change is evident in either charge or spin for third-layer Fe atoms due to the static natures of adsorbed N in the trough region. We conclude that spin pairing on the Fe(211) surface may play an important role in future design for catalysts to improve the efficiency of the Haber-Bosch process. Further research is required in this area to fully explore the importance of spin in the $NH_3$ pathway.

**Table 1** – Magnetic moment changes across primary reaction barrier. As seen in prior research, magnetic moment decreases as number of valence bonds formed on surface increase (from dissociation of $N_2$ -> 2N in this case). Change in magnetic moment relative to blank Fe(211)R surface is also shown.

| Species | Total Mag. Moment (μB) | ΔMag |
|---|---|---|
| (211)R surface | 55.550 | 0.00 |
| 2N-$N_2$ | 51.347 | -4.203 |
| (TS) 2N-$N_2$ -> 4N initial | 49.426 | -6.124 |
| 4N initial | 48.040 | -7.51 |

## Kinetics and comparison with experiment

The Fe(111) and Fe(211) surface have been widely researched[6,23,29] through experimental means, including Temperature-Programmed Desorption using Low-Energy Electron Diffraction (LEED).[29] Experimental work has shown that the Fe(211) surface assumes the missing row reconstruction in the presence of hydrogen at standard temperatures and pressures.[9,10] Prior experimental work at T = 673K P = 20 atm (total) found that the Fe(211) surface leads to a $NH_3$ synthesis rate of around ~25% less than the Fe(111) surface in the limit of zero ammonia pressure (actual ammonia pressures were undisclosed).[6]

View Article Online
DOI: 10.1039/C9CP01611B



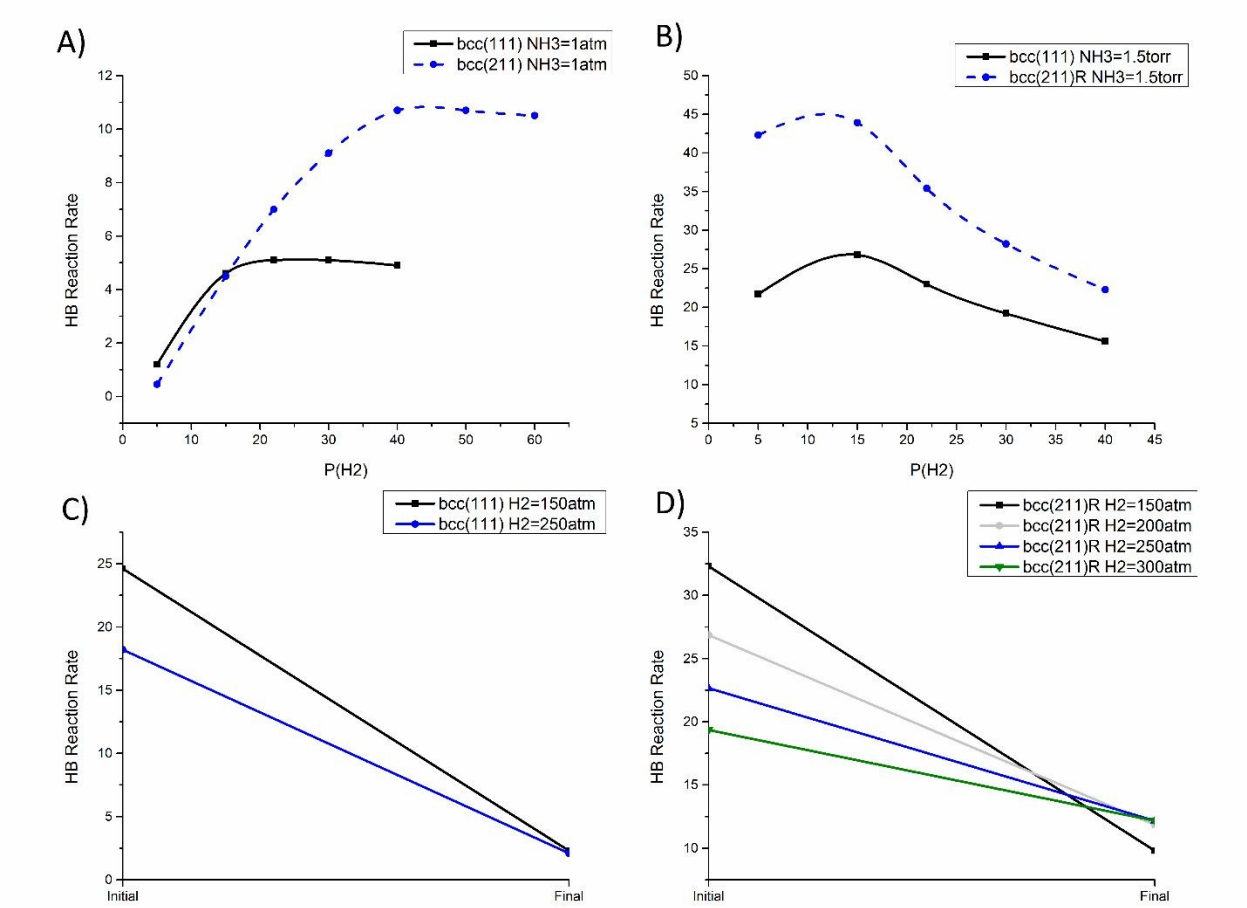


**Fig. 4 -** HB reaction rates over Fe(111) and Fe(211)R surface catalysts under steady-state conditions of ammonia synthesis as predicted by kMC simulations at 673 K and various $H_2$, $N_2$, $NH_3$ pressures using QM data: (A) HB rates over Fe(111) and Fe(211)R surfaces as functions of $P(H_2)$ keeping $P(N_2)$=5 atm, $P(NH_3)$=1 atm; (B) HB rates over Fe(111) and Fe(211)R surfaces as functions of $P(H_2)$ keeping $P(N_2)$=5 atm, $P(NH_3)$=1.5 torr; (C,D) HB rates over Fe(111) (C) and Fe(211)R (D) at high overall pressure under initial conditions (i.e., $P(H_2)$ as indicated in the inset, $P(N_2)$=50 atm, $P(NH_3)$=1 atm) and final conditions (i.e., $P(H_2)$ as indicated in the inset, $P(N_2)$=40 atm, $P(NH_3)$=20 atm). Rates expressed as $NH_3$ molecules produced per (2x2) unit cell per sec.

We now focus on the kinetics of HB process on Fe(211)R in comparison with Fe(111). Results of kMC simulations are reported below. Then, we analyze and interpret these results via a simplified kinetic model, and finally we introduce a generalized Wulff construction under steady-state and compare with experiment.

## kMC Simulations

We used the QM-derived free-energy diagram discussed above to predict HB reaction rates under steady-state conditions via a kinetic Monte Carlo (kMC) approach[40] following the same procedure employed in previous research[9]: the kMC rates are calculated using transition state theory (TST)[41] as $(k_BT/h)\exp(-\Delta G^{\dagger}/k_BT)$, where $\Delta G^{\dagger}$ is the difference in free energy between the starting state and the saddle point. These rates are also calculated with the specification that in the case of ER reactions involving gas-phase species turning into adsorbates we use TST for the

View Article Online
DOI: 10.1039/C9CP01611B



reverse LH process, and we invoke microscopic reversibility principle to calculate the rate of the direct process. In the kMC runs, we used 20 independent replicas and $2 \times 10^{10}$ kMC steps (30 minutes) in each replica, testing that the results so produced are converged within 2% in the production rate.

**Table 2.** Percent of populations (i.e., residence times) = ti(%) for the most relevant configurations in (2x2) unit cells of the Fe(111) and Fe(211)R surfaces under steady-state of ammonia synthesis as predicted by kMC simulations at 673 K and various $H_2$, $N_2$, $NH_3$ pressures using QM data. All other populations are below 1%, except 2N_z.2H (and also to a lesser extent 4N and 3N.H) for Fe(111) which make up for the missing percent to 100%. Pressure in atmospheres.

| | $p(H_2,N_2,NH_3)=(15,5,1)$ **– (111)** | | $p(H_2,N_2,NH_3)=(15,5,1)$ – **(211)R** |
|---|---|---|---|
| configuration | $t_i$ (%) | configuration | $t_i$ (%) |
| $3N.NH_2$ | 23.13 | 2N.NH.2H | 42.82 |
| $2N_{\_z}.NH_2.H$ | 52.63 | 3N.NH.H | 28.21 |
| $2N_{\_z}.NH_2.2H$ | 6.88 | 4N** | 5.42 |
| $2N_{\_f}.2H$ | 7.06 | 2N.4H | 22.81 |
| | $p(H_2,N_2,NH_3)=(40,5,1)$ **– (111)** | | $p(H_2,N_2,NH_3)=(40,5,1)$ – **(211)R** |
| configuration | $t_i$ (%) | configuration | $t_i$ (%) |
| $3N.NH_2$ | 3.76 | 2N.NH.2H | 42.96 |
| $2N_{\_z}.NH_2.H$ | 55.12 | 3N.NH.H | 6.63 |
| $2N_{\_z}.NH_2.2H$ | 11.76 | 4N** | 11.33 |
| $2N_{\_f}.2H$ | 20.59 | 2N.4H | 38.15 |
| | $p(H_2,N_2,NH_3)=(250,50,1)$ **– (111)** | | $p(H_2,N_2,NH_3)=(250,50,1)$ – **(211)R** |
| configuration | $t_i$ (%) | configuration | $t_i$ (%) |
| $3N.NH_2$ | 0.41 | 2N.NH.2H | 5.30 |
| $2N_{\_z}.NH_2.H$ | 23.91 | 3N.NH.H | 1.09 |
| $2N_{\_z}.NH_2.2H$ | 12.76 | 4N** | 3.84 |
| $2N_{\_f}.2H$ | 47.83 | 2N.4H | 88.96 |
| | $p(H_2,N_2,NH_3)=(15,5,1.5t)$ **– (111)** | | $p(H_2,N_2,NH_3)=(15,5,1.5t)$ – **(211)R** |
| configuration | $t_i$ (%) | configuration | $t_i$ (%) |
| $3N.NH_2$ | 9.14 | 2N.NH.2H | 3.10 |
| $2N_{\_z}.NH_2.H$ | 28.53 | 3N.NH.H | 8.51 |
| $2N_{\_z}.NH_2.2H$ | 3.73 | 4N** | 58.21 |
| $2N_{\_f}.2H$ | 41.57 | 2N.4H | 27.91 |

We focused on reaction conditions around $P(H_2)$ = 15 atm, $P(N_2)$ = 5 atm, $P(NH_3)$ = 1 atm, and T=673 K, which are realistic target operating conditions for a less energy-demanding HB process, but we also investigated a broader set of pressures to be able to compare with

View Article Online
DOI: 10.1039/C9CP01611B



experiments conducted at low $P(NH_3)$ of 1.5 torr[6] and because we found that a stoichiometric ratio of reactants can be non-optimal for the Fe(211)R surface (a complete set of HB rate results can be found in Table S2 of the SI). The free-energy diagram at low $P(NH_3)$ of 1.5 torr is displayed in Fig. S11 of SI. In order to achieve an unbiased comparison between the Fe(111) and Fe(211)R catalysts, we used an analogous set of configurations and identical numerical parameters for these 2 systems: 24 equilibrium and 29 transition states for Fe(211)R, 21 equilibrium and 26 transition states for Fe(111) (for the latter, we streamlined the original set of 26 equilibrium and 49 transition states[10] by neglecting some $H_2$-adsorption side-processes).

Representative results are reported in Fig. 4, Table 2, and Table S2 of the SI. In Fig. 4(a) we kept $P(N_2)$ = 5 atm and $P(NH_3)$ = 1 atm fixed, and varied $P(H_2)$ in the range 5-50 atm. The turn-over-frequency (TOF) for Fe(111) and Fe(211)R catalysts exhibit a quite different behavior as a function of $P(H_2)$: Fe(111) is only slightly dependent on hydrogen pressure (achieving a shallow maximum in $P(H_2)$ between 22 and 30 atm, only 10% greater than that achieved under stoichiometric conditions at 15 atm), whereas on Fe(211)R HB reaction rate can be more than doubled by increasing $P(H_2)$ from 15 to 40 atm. At variance, Fig. 4(b) shows that the optimal $H_2$:$N_2$ reactant ratio is stoichiometric at very low $P(NH_3)$ pressure, i.e. $P(NH_3)$ = 1.5 torr, for Fe(111) and nearly stoichiometric for Fe(211)R. In Fig. 4(c) we finally report rate results in the high-pressure régime, i.e., similar to the actual industrial conditions of the HB process which is typically held at 200 atm of total reactant pressure, by plotting rates at initial [$P(NH_3)$ = 1 atm] and final [$P(NH_3)$ = 20 atm] conditions. We found that for Fe(111) the optimal reactant ratio is stoichiometric also under these conditions and the ammonia poisoning effect is severe (the rate decreases by a factor of 10 between initial and final conditions). In contrast, we found that for Fe(211)R the optimal reactant ratio is stoichiometric under these conditions, but the ammonia poisoning effect is reduced, and the ammonia production rate decreases only by a factor of ≈3 between initial and final conditions at very high pressures, i.e. from 22.6 $NH_3$ molecules per second per (2x2) site at $P(H_2)$ = 250 atm, $P(N_2)$ = 50 atm, $P(NH_3)$ = 1 atm to 12.2 $NH_3$ molecules/sec/(2x2) at $P(H_2)$ = 220 atm, $P(N_2)$ = 40 atm, $P(NH_3)$ = 20 atm. These results will be rationalized in the next subsection.

Finally, in Table 2 we report per-cent populations (i.e., per-cent residence times) for few most relevant configurations in a (2x2) unit cell under steady-state of ammonia synthesis as predicted by our kMC approach for Fe(111) and Fe(211)R catalysts. In particular, we investigated conditions of both moderate total pressure and two $H_2$ pressures: $P(N_2)$ = 5 atm, $P(NH_3)$ = 1 atm, and $P(H_2)$ = 15 atm or $P(H_2)$ = 40 atm, and high total pressure: $P(H_2)$ = 250 atm, $P(N_2)$ = 50 atm, $P(NH_3)$ = 1 atm (temperature is always T=673°K). It is clear from Table 2 that significant shifts in populations occur by varying the reaction conditions. For Fe(111) this typically corresponds to a depopulation of the 3N.$NH_2$ state and a population of the 2N_f.2H state by increasing $H_2$ or total pressure. For the Fe(211)R catalyst the 2N.NH.2H configuration basically loses weight in favor of the 2N.4H configuration, in which at high total pressure the system resides for more than 92% of the time. These phenomena will be rationalized below, and the populations will be used in the steady-state Wulff construction below.

**Kinetic analysis**

Here we interpret the above kMC results via a simplified kinetic model based on the evolution of the QM free-energy diagram under different conditions.

View Article Online
DOI: 10.1039/C9CP01611B



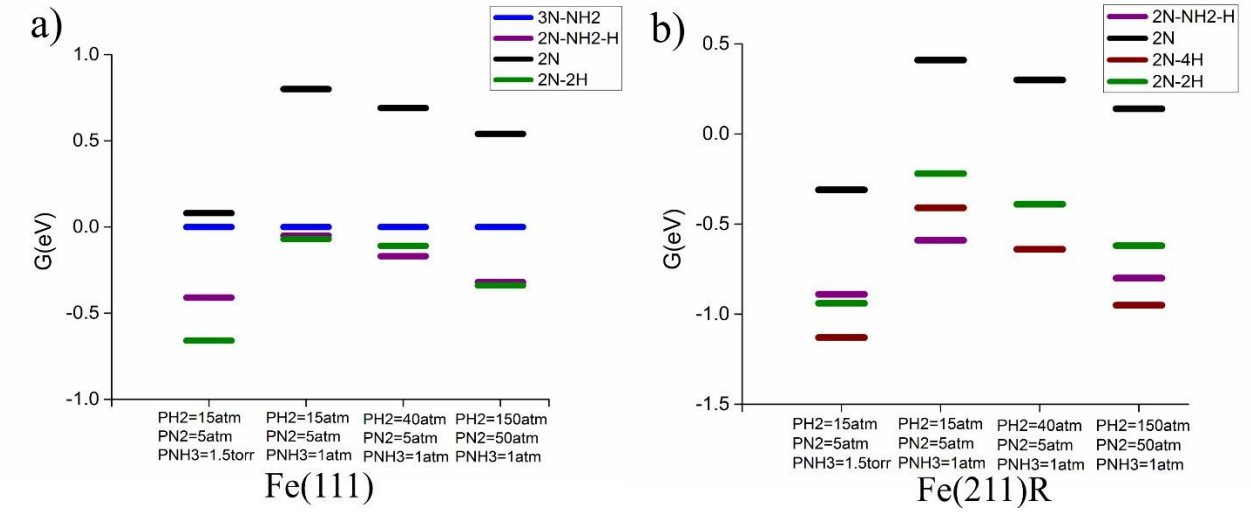


**Fig. 5 -** Relative free-energies (G) of selected configurations over Fe(111) (left panel) and Fe(211)R (right panel) surfaces under different conditions of ammonia synthesis, conditions shown below axis. In the left panel, 2N.NH2.H stands for $2N\__i.NH_2.2H$, while 2N.2H stands for $2N\__i.2H$. The $3N.NH_2$ configuration is taken as reference, with a free energy of zero. Free-energies in eV.

The cyclic reaction network with energy barriers highlighted with a blue line in Fig. 2 corresponds to the shortest (minimum-barrier) path on the given catalyst. Here we determined this shortest path heuristically but for any given reaction network it can be determined using the Dijkstra's algorithm[42].

Along this reaction path we first single out two key states: (i) the state realizing the minimum in free-energy (we can call it "dynamical resting state") and (ii) the highest successive transition state along the path (highest saddle point). We then approximate the overall rate as: $(k_BT/h)\exp(-\Delta G^{\dagger}/k_BT)$, where $\Delta G^{\dagger}$ is the difference in free-energy between the dynamical resting state and the highest saddle point.

Note that varying the pressure conditions can change the dynamical resting state and/or the highest saddle point. Indeed, for both Fe(111) and Fe(211)R there is a switch in resting state between intermediate and high total pressure or very low ammonia pressure conditions. This is illustrated in Fig. 5: for Fe(111) the resting state changes from $2N.NH_2.H$ to 2N.2H, while for Fe(211)R the resting state from 2N.NH.2H to 2N.4H configurations, respectively. Moreover, for Fe(111) there is an additional switch in the highest saddle point by varying the ammonia pressure: at low $P(NH_3)$ the rate-determining transition state is a hydrogen migration step (i.e., the step "$3N.NH_2.2H \rightarrow 3N.NH_3.H$"), whereas at high $P(NH_3)$ it is $N_2$ adsorption onto the $2N\__i$ state (i.e., the step "$2N\__i + N_2 \rightarrow 2N\__i.N_2$").

To better clarify this point, we refine our analysis, and note that along the Dijkstra's path we can single out not just the absolute minimum, but all the states realizing a deep minimum in free-energy. These states partition the path into successive sections. In each of these section, defined by an initial and final state, we then single out the highest-energy transition state. Within this picture, we use a simplified kinetic model, in which the forward rate from the initial to the final state within each section of the catalytic path (say – the K-th) can be approximated as: $(k_BT/h)\exp(-(G_K^{\dagger}-G_K^{i})/k_BT)$, where $G_K^{\dagger}$ is free-energy of the highest transition state and $G_K^{i}$ is free-energy of the initial state in the K-th section [analogously the backward rate can be

View Article Online
DOI: 10.1039/C9CP01611B



approximated as: $(k_BT/h)\exp(-(G_K^{\dagger}- G_K^{f})/k_BT)$, where $G_K^{f}$ is free-energy of the final state in the section]. $\Delta G_K^{\dagger} = G_K^{\dagger}-G_K^{i}$ is then the effective free-energy barrier associated with the given (K-th) section into which we have partitioned the Dijkstra's path. By changing the pressures (i.e., the chemical potential of gas-phase species) the relative position of the various initial/final states and of the corresponding saddle points can change, and thus also the relative magnitude of the free-energy barriers $\Delta G_K^{\dagger}$, with the possibility of a switch between two $\Delta G_K^{\dagger}$ as the largest barrier. A change in the nature of the highest (rate-determining) barrier can therefore occur. Indeed for HB on Fe Fe(111) we have two main local minimum configurations in the free-energy profile at $P(H_2)$ = 15 atm and $P(N_2)$ = 5 atm pressures: $3N.NH_2$ and $2N.NH_2.H$ (with 2N.NH2.H competing with 2N.2H). In the «$3N.NH_2 \rightarrow 2N.NH_2.H$» section of the reaction path, the highest transition state is associated with a hydrogen migration step: "$3N.NH_2.2H \rightarrow 3N.NH_3.H$", whereas in the «$2N.NH_2.H \rightarrow 3N.NH_2.2H$» section, the highest transition state is associated with a nitrogen adsorption step: "$2N\__j + N_2 \rightarrow 2N\__j.N_2$". Now, by reducing ammonia pressure, the free-energy difference between the $2N.NH_2.H$ and 2N configurations decreases, and therefore also the barrier of the «$2N.NH_2.H \rightarrow 3N.NH_2.2H$» section of the path, so much as to become smaller than the barrier of the «$3N.NH_2 \rightarrow 2N.NH_2.H$» section of the reaction path, which is independent of ammonia pressure, thus explaining the change in the highest saddle point at low $P(NH_3)$. A qualitatively similar switch also occurs on Fe(211)R, where the barrier of the «$4N^{**} \rightarrow 3N.NH.H$» section becomes rate-determining at very low ammonia pressure thus explaining why Fe(211)R is less active than Fe(111) under these conditions, in agreement with experimental data. [6]

To conclude this section, we note that:

(i) From this analysis it results that the evolution of the reaction rate as a function of pressure conditions corresponds to a piece-wise linear function (thus with a discontinuous first derivative – continuity is recovered by introducing the full kMC kinetics into the model or by introducing a two-state model at the crossing point between two régimes)

(ii) The present analysis provides the basis of a protocol for a rational design of improved ammonia synthesis catalysts via Hierarchical High-Throughput Screening (HHTS), previously applied to Fe(111)[43] and now applicable also to the even more promising Fe(211)R catalyst surface.

**Comparison with experiment and Wulff construction under steady-state**

Experimentally, a comparison between the catalytic activity of well-defined single crystal Fe surfaces in the HB process has been reported by Strongin et al.[6] According to this study, under conditions of temperature T = 673 K, $P(H_2)$ = 15 atm, $P(N_2)$ = 5 atm, and asymptotically zero $P(NH_3)$ pressure, the HB production rate per unit area on the Fe(211) surface is 25% smaller than on the Fe(111) surface. In these experiments no information was available on whether the Fe(211) surface was reconstructed or not and the actual $P(NH_3)$ pressure was not disclosed. Our prediction is a TOF of 26.8 $NH_3$ molecules per (2x2) unit cell per second on Fe(111), and 18.7 $NH_3$ molecules per (2x2) unit cell per second on Fe(211)R, respectively, under conditions of temperature T = 673 K, $P(H_2)$ = 15 atm, $P(N_2)$ = 5 atm, and $P(NH_3)$ = 1.5 torr. By considering the different areas of the (2x2) unit cells of 54.6 $Å^2$ for Fe(111) and 38.6 $Å^2$ for Fe(211), one obtains that the catalytic activity per area of Fe(211)R is 99% that of Fe(111), a ratio which increases to 105% when increasing ammonia pressure to 1 atm. Thus, our predictions are within

View Article Online
DOI: 10.1039/C9CP01611B



a factor of 0.75 from experiment, which is an excellent accuracy considering that the two surfaces and the associated reaction mechanisms are very different, the idealized conditions assumed in our modeling and the limitations of QM/DFT energetics. To be fully rigorous, in predicting actual rates we also need to estimate which fraction of Fe(211) is reconstructed under reaction conditions. We assume that the ratio of the populations between reconstructed and unreconstructed surfaces equals the Boltzmann factor of the difference in their surface free-energies under the given conditions. However, here we account for the fact that the system is under dynamic conditions (steady-state but out-of-equilibrium) by evaluating surface energies as a weighted average of the free-energies of the individually populated configurations in the diagram of Figure 2. Such an average takes into account how the configurations are actually populated, i.e., assuming weights equal to the populations derived from the kMC simulations – see Table 2. In the present case this more rigorous estimate of surface energy does not change qualitatively the net result, since we find that the Fe(211)R surface is still favorable under HB steady state at 20 atm and very low ammonia pressure. We also find that the Fe(211)R surface has a surface energy lower than that of the (111) surface. We find in fact that the bare surface energies of 0.178 eV/Å$^2$ and 0.181 eV/Å$^2$ for Fe(111) and Fe(211)R, respectively, become 0.139 eV/Å$^2$ and 0.127 eV/Å$^2$, respectively, under steady-state HB reaction (at 673 K). Full surface energy data calculated with the PBE-D3 functional is included in Table S3 of the SI.

We note in passing that the present approach to evaluate surface energies under reactive conditions can be applied, by combining dynamic and thermodynamic reasoning, to define a generalized Wulff construction or a Wulff construction under steady-state (or 'dynamic' Wulff construction.) In the Wulff construction, the thermodynamic minimum-energy shape of a particle is the one in which the distance of each given facet from the particle center is inversely proportional to the surface energy of the facet.[44] We propose that surface energies are not evaluated statically but as a sum of adsorbate-configuration free energies weighted by the corresponding steady-state (kMC) populations (modified Wulff constructions have been introduced for a long time in the theory of crystal growth.) [45] The calculated Wulff shape using this approach is presented in Fig. S13, including a comparison with previously calculated surface energy values.[46] We find reasonable agreement with the previously determined Wulff shape by Tran et. al,[46] with some variance in surface energy values due to the difference in functionals used. It will be interesting to check and validate these predictions in future experimental work.

## CONCLUSIONS

We reported the first full explanation of the reaction mechanism for ammonia synthesis on the Fe(211) missing row reconstructed surface including 24 main pathway states and 29 transition states. Four primary processes were found to play an important role in the reaction pathway: a Langmuir-Hinshelwood mechanism of hydrogenation to produce $NH_x$ species, $NH_3$ desorption to the gas phase, $N_2$ adsorption, and $N_2$ dissociation which last – at variance with the Fe(111) surface – here has by far the largest barrier and represents the rate-determining step. The overall energy barrier for the reaction pathway was determined to be 1.59 eV at 20 atm total reactant pressure and low $NH_3$ pressure (1.5 Torr).

The QM results were used in a kinetic Monte Carlo modeling to obtain reaction rates which has been compared against experimental data[4] finding an excellent agreement, with the experimental ratio between rates on Fe(211) and Fe(111) surfaces at 20 atm total reactant pressure in the limit

View Article Online
DOI: 10.1039/C9CP01611B



of zero ammonia pressure of 0.75 comparing with a 0.99 ratio between rates on Fe(211)R and Fe(111) from our modeling at 20 atm total reactant pressure and 1.5 torr ammonia pressure. This excellent agreement on two very different surfaces and reaction mechanisms is a testament of the accuracy of our modeling, and opens the way to a deeper understanding and rational design of improved catalysts. Especially noteworthy is the fact that the HB catalytic activity of Fe(211)R is comparable with that of Fe(111) at low ammonia pressure, in agreement with available experimental data, but becomes significantly larger in a wide range of conditions, particularly in conditions close to the industrial ones. This result, combined with the fact that the steady-state surface energy of Fe(111) is higher than that of Fe(211)R which is therefore predicted to be more abundant on the basis of a dynamic Wulff construction, leads us to suggest that (211)R is the dominant catalytically active phase, at variance with catalytic studies at low conversion.[6] This supports the view of a complex surface structure for the industrial catalyst as proposed in previous research.[2] Moreover, the striking difference in structure and reaction mechanisms between these two most active Fe surfaces suggests that it would be fruitful to search for alternative and possibly complementary materials (e.g., dopants) to increase the HB catalytic activity of these systems.[42]

Comparison of changes in spin and charge during the states associated with the primary reaction barrier indicates a correlation between spin coupling between surface Fe and adsorbed species to form valence bonds during dissociation and movement of those species. Spin decreases and the corresponding charge increases were noted for the Fe atoms involved in such bonding during the transition and resulting states, suggesting a spin analysis to increase catalytic efficiency by searching for doping metals having localized spins. A natural future development of this work is combining this insight with Hierarchical High-Throughput Screening protocols[39] to design novel HB catalysts ideally working under much milder conditions than those presently employed.

## ELECTRONIC SUPPLEMENTARY INFORMATION (ESI)

ESI is available containing detailed geometry and potential energy curves for all main pathway transition states, detailed geometry and potential energy curves for the alternate pathway transition states for barrier minimization, detailed information on surface energy calculations and surface reconstruction comparisons, free energy diagram for 673 K, 20 atm low pressure state ($P(NH_3)$ = 1.5 torr), comparison of preferred position and bond lengths for adsorbed species on Fe(211) and Fe(211)R , Comparison of HB catalytic reaction rates under steady-state conditions on (2x2) unit cells of the Fe(111) and Fe(211)R surfaces, and full information for electronic and free energies of all synthesis pathway states using the PBE-D3 functional at both 673 K. Small molecule thermodynamic information and full information on the kMC calculations are also available in xsl file.

## AUTHORS CONTRIBUTIONS

AF, WAG and QA designed the strategy of this work. JF and QA performed QM calculations. AF performed kMC simulations. All authors wrote the paper.

View Article Online
DOI: 10.1039/C9CP01611B



**CORRESPONDING AUTHORS**

*E-mail: qia@unr.edu (Qi An).

*E-mail: wag@wag.caltech.edu (William A. Goddard, III).

*E-mail: alessandro.fortunelli@cnr.it (Alessandro Fortunelli)

**ORCID**

Jon Fuller: 0000-0003-1233-7842

Alesandro Fortunelli: 0000-0001-5337-4450

William A. Goddard, III: 0000-0003-0097-5716

Qi An: 0000-0003-4838-6232

**CONFLICTS OF INTEREST**

The authors declare no competing financial interest.

**ACKNOWLEDGEMENTS**

This work was supported by the U.S. Department of Energy (USDOE), Office of Energy Efficiency and Renewable Energy (EERE), Advanced Manufacturing Office Next Generation R&D Projects under contract no. DE-AC07-05ID14517 (program manager Dickson Ozokwelu, in collaboration with Idaho National Laboratories, Rebecca Fushimi). A.F. gratefully acknowledges financial support from a Short-Term Mission (STM) funded by Italian Consiglio Nazionale delle Ricerche (CNR). We would like to thank the Information Technology department at the University of Nevada, Reno for computing time on the High Performance Computing Cluster (Pronghorn). Some calculations were also carried out on a GPU-cluster provided by DURIP (Cliff Bedford, program manager).

**REFERENCES**

(1) U.S. Geological Survey. Mineral commodity summaries 2018. *Mineral Commodity Summaries*, 2018.

(2) R. Schlögl, Catalytic synthesis of ammonia – a "never-ending story"? *Angew. Chem., Int. Ed.*, 2003, **42**, 2004−2008

(3) A. Mittasch and W. Frankenburg, Early studies of multicomponent catalysts, *Adv. Catal.,* 1950, **2**, 81−104

(4) N.D. Spencer, R.C. Schoonmaker, and G.A. Somorjai, Iron single crystals as ammonia synthesis catalysts: effect of surface structure on catalyst activity, *J. Catal.,* 1982, **74**, 129–135

(5) G. Ertl, Primary steps in catalytic synthesis of ammonia, *Journal of Vacuum Science & Technology A*, 1983, **1**, 1247–1253

View Article Online
DOI: 10.1039/C9CP01611B



(6) G.A. Somorjai and N. Materer, Surface Structures in Ammonia Synthesis, *Top. Catal.* 1994, **1**, 215−231

(7) K. Kolanski, Surface Science: Foundations of Catalysis and Nanoscience, John Wiley and Sons, Hoboken, NJ, 2012.

(8) J. Zhang, F. Ma, and K. Xu, Calculation of the surface energy of bcc metals by using the modified embedded-atom method, *Surf. Interface Anal.,* 2003, **35***,* 662-666

(9) X. Lin, J. Chen, J. Wang, and W. Huang, First-principles study of the relaxation and energy of bcc-Fe, fcc-Fe and AISI-304 stainless steel surfaces, *Appl. Surf. Sci.,* 2009, **255**, 9032-9039

(10) J. Qian, Q. An, A. Fortunelli, R.J. Nielsen, and W.A. Goddard, Reaction Mechanism and Kinetics for Ammonia Synthesis on the Fe(111) Surface, *J. Am. Chem. Soc.*, 2018, **140**, 6288–6297

(11) J.P. Perdew, K. Burke and M. Ernzerhof, Generalized gradient approximation made simple, *Phys. Rev. Lett.,* 1996, **77**, 3865−3868

(12) J.P. Perdew, K. Burke, and M. Ernzerhof, Coupling-constant dependence of atomization energies, *Phys. Rev. Lett*., 1997, **78**, 1396

(13) E.R. Johnson and A.D. Becke, A post-Hartree-Fock model of intermolecular interactions: Inclusion of higher-order corrections, *J. Chem. Phys.,* 2006, **124**, 174104

(14) G. Kresse and J. Hafner, Ab initio molecular dynamics for liquid metals, *Phys. Rev. B,* 1993, **47**, 558-561.

(15) G. Kresse and J. Hafner, Ab initio molecular-dynamics simulation of the liquid-metal–amorphous-semiconductor transition in germanium, *Phys. Rev. B*, 1994, **49**, 14251-14269

(16) G. Kresse and J. Furthmüller, Efficiency of ab-initio total energy calculations for metals and semiconductors using a plane-wave basis set, *Comput. Mater. Sci.*, 1996*,* **6**, 15-50

(17) G. Kresse, and J. Furthmüller, Efficient iterative schemes for ab initio total-energy calculations using a plane-wave basis set, *Phys. Rev. B.* 1996, **54**, 11169-11186

(18) G. Henkelman, B.P. Uberuaga, and H. Jónsson, A climbing image nudged elastic band method for finding saddle points and minimum energy paths, *J. Chem. Phys.* 2000, **113**, 9901–9904

(19) E. Kampshoff, N. Waelchli, A. Menck, and K. Kern, Hydrogen-induced missing-row reconstructions of Pd(110) studied by scanning tunneling microscopy, *Surf. Sci*., 1996, **360**, 55–60

(20) G.A. Somorjai and N. Materer, Surface structures in ammonia synthesis, *Top. Catal.* 1994, **1**, 215−231

View Article Online
DOI: 10.1039/C9CP01611B



(21) A. Vojvodic, A.J. Medford, F. Studt, F. Abild-Pedersen, T.S. Khan, T. Bligaard, and J.K. Nørskov, Exploring the limits: A low-pressure, low-temperature Haber–Bosch process, *Chem. Phys. Lett.,* 2014, **598**, 108–112

(22) T. Wang, X. Tian, Y. Yang, Y-W. Li, J. Wang, M. Beller, and H. Jiao, Coverage-Dependent N2 Adsorption and Its Modification of Iron Surfaces Structures, *J. Phys. Chem. C.*, 2016, **120**, 2846-2854

(23) T. Wang, S. Wang, Q. Luo, Y-W. Li., J. Wang, M. Beller, and H. Jiao, Hydrogen Adsorption Structures and Energetics on Iron Surfaces at High Coverage, *J. Phys. Chem. C.,* 2014, **118**, 4181-4188

(24) H. McKay, S. Jenkins, and D. Wales, Theory of NHx ± H Reactions on Fe{211}, *J. Phys. Chem. C.,* 2009, **113**, 15274-15287

(25) R.J. Baxter and P. Hu, Insight into why the Langmuir-Hinshelwood mechanism is generally preferred, *J. Chem. Phys.,* 2002, **116**, 4379–4381

(26) H. Hidaka, M. Watanabe, A. Kouchi, and N. Watanabe, FTIR study of ammonia formation via the successive hydrogenation of N atoms trapped in a solid N2matrix at low temperatures, *Phys. Chem. Chem. Phys.*, 2011, **13**, 15798–15802

(27) N.D. Spencer, R.C. Schoonmaker, and G.A. Somorjai, Iron single crystals as ammonia synthesis catalysts: effect of surface structure on catalyst activity, *J. Catal.,* 1982, **74**, 129–135

(28) W. Arabczyk, I. Jasińska, and K. Lubkowski, The surface properties of iron catalyst for ammonia synthesis, *React. Kinet. Catal. L.*, 2004, **83**, 385–392

(29) E. Hassold, U. Löffler, R. Schmiedl, M. Grund, L. Hammer, K. Heinz, and K. Müller, Hydrogen induced missing row reconstruction of Fe (211), *Surf. Sci.*, 1995, **326**, 93–100

(30) R. Schmiedl, W. Nichtl-Pecher, K. Heinz, K. Müller, and K. Christmann, Hydrogen on Fe (211): commensurate and reconstructed phases, *Surf. Sci.,* 1990*,* **235**, 186–196

(31) L.P. Nielsen, F. Besenbacher, E. Laegsgaard, and I. Stensgaard, Nucleation and of a H-induced reconstruction of Ni(110) *Physical Review B.,* 1991, **44**, 13156–13159

(32) M.M. Rodriguez, E. Bill, W. Brennessel, and P. Holland, N2 reduction and hydrogenation to ammonia by a molecular iron-potassium complex, *Science*, 2011, **334***,* 780-783

(33) S. Bare, D.R. Strongin, and G.A. Somorjai, Ammonia synthesis over iron single-crystal catalysts: the effects of alumina and potassium, *J. Phys. Chem.,* 1986, **90**, 4726–4729

(34) H.B. Chen, J.D Lin, Y. Cai, X.Y. Wang, J. Yi, J. Wang, and D.W. Liao, Novel multi-walled nanotubes-supported and alkali-promoted Ru catalysts for ammonia synthesis under atmospheric pressure, *Appl. Surf. Sci.*, 2001, **180**, 328–335

(35) W. Raróg-Pilecka, E. Miśkiewicz, D. Szmigiel, and Z. Kowalczyk, Structure sensitivity of ammonia synthesis over promoted ruthenium catalysts supported on graphitised carbon, *J. Catal.*, 2005, **231**, 11–19

View Article Online
DOI: 10.1039/C9CP01611B



(36) J. Kua and W.A. Goddard, Chemisorption of organics on Platinum. 1. The interstitial electron model, *J. Phys. Chem. B.*, 1998, **102**, 9481−9491

(37) J. Kua, and W.A. Goddard, Chemisorption of Organics on Platinum. 2. Chemisorption of C2Hx and CHx on Pt(111), *J. Phys. Chem. B.*, 1998, **102**, 9492−9500.

(38) J. Kua, F. Faglioni, and W.A. Goddard, Thermochemistry for Hydrocarbon Intermediates Chemisorbed on Metal Surfaces: CHn-m(CH3)m with n = 1, 2, 3 and m ≤ n on Pt, Ir, Os, Pd, Rh, and Ru, *J. Am. Chem. Soc.*, 2000, **122**, 2309−2321

(39) J. Kua, and W.A Goddard, Oxidation of methanol on 2nd and 3rd row group VIII transition metals (Pt, Ir, Os, Pd, Rh, and Ru): application to direct methanol fuel cells, *J. Am. Chem. Soc.*, 1999, **121**, 10928− 10941

(40) D.T. Gillespie, A General Method for Numerically Simulating the Stochastic Time Evolution of Coupled Chemical Reactions, *J. Comput. Phys*., 1976, **22**, 403–434

(41) G.H. Vineyard, Frequency factors and isotope effects in solid state rate processes, *J. Phys. Chem. Solids,* 1957, **3**, 121–127

(42) E.W. Dijkstra, A note on two problems in connection with graphs, *Numer. Math.,* 1959, **1**, 269–271

(43) Q. An, Y.D. Shen, A. Fortunelli, and W.A Goddard III, QM-mechanism-based hierarchical high-throughput in silico screening catalyst design for ammonia synthesis, *J. Am. Chem. Soc.,* 2018, **140**, 17702-17710

(44) G. Wulff, On the question of speed of growth and dissolution of crystal surfaces, *Z. Krystallogr.,* 1901, **34**, 449-530

(45) A.A. Chernov, The kinetics of the growth forms of crystal, *Sov. Phys. Crystallogr.*, 1963, **7**, 728-730

(46) Tran, R., Xu, Z., Radhakrishnan, B., Winston, D., Sun, W., Persson, K., and Ong, S. P. Surface energies of elemental crystals, *Sci. Data,* 2016, **3:**160080**.**

View Article Online
DOI: 10.1039/C9CP01611B



## Graphical Abstract